Earth Surf. Dynam. Discuss., https://doi.org/10.5194/esurf-2018-35
Manuscript under review for journal Earth Surf. Dynam.
Discussion started: 3 May 2018

Clast imbrications in coarse-grained sediments suggest changes from upper to lower flow regime conditions

Fritz Schlunegger, Philippos Garefalakis
Institute of Geological Sciences
University of Bern, Switzerland
fritz.schlunegger@geo.unibe.ch
philippos.garefalakis@students.unibe.ch

Abstract

Clast imbrications are presumably the most conspicuous sedimentary structures in coarse-grained clastic deposits. In this paper, we test whether the formation of such a fabric is related to changes from lower to upper flow regime conditions in streams. To this extent, we calculate the Froude number at the incipient motion of coarse-grained bedload for various values of relative bed roughness and stream gradient. We then compare the results with data from modern streams and stratigraphic records. The calculations show that upper flow regime conditions most likely establish where average stream gradients exceed c. 0.5±0.1°, and where relative bed roughness values are larger than ~0.06±0.01. Similarly, data from modern streams reveal that imbricated clasts are found where channels are steeper than c. 0.5±0.2°, and where relative bed roughness values exceed ~0.07. Likewise, imbricated conglomerates are encountered in late Oligocene foreland basin sequences where paleo-slopes were greater than 0.4°. We use these relationships to propose that clast imbrications occur where channel gradients exceed a threshold, which appears large enough for upper flow regime conditions to establish. We finally relate the formation of an imbricated arrangement of clasts to a mechanism where material transport occurs through rolling, or pivoting. This process requires a large shear force and thus a large flow velocity upon transport, which is likely to be associated with shifts from the lower to the upper flow regime. Our results thus suggest that clast imbrications are suitable recorders of upper flow regime conditions upon sediment transport.

Introduction

Conglomerates, representing the coarse-grained spectrum of clastic sediments, bear key information about the provenance of the material (Matter, 1964), the environment in which these sediments were deposited (Rust, 1978; Middleton and Trujillo, 1984), and the hydro-climatic conditions upon transport and deposition of the sediments (Duller et al., 2012; D'Arcy et al., 2017). Conglomerates display the entire range of possible sedimentary structures including a massive-bedded fabric, cross-beds and

Earth Surf. Dynam. Discuss., https://doi.org/10.5194/esurf-2018-35
Manuscript under review for journal Earth Surf. Dynam.
Discussion started: 3 May 2018

horizontal stratifications. However, the most striking features are clast imbrications (Figure 1), which refer to a depositional fabric where clasts overlap each other, similar to a run of toppled dominoes (e.g., Pettijohn, 1957; Yagishita, 1997; Rust, 1984; Potsma and Roep, 1985; Todd, 1996). In the past decades, the occurrence of clast imbrications in streams has been considered as primary recorders of high stage flows (Rust, 1978; Miall, 1978; Sinclair and Jaffey, 2001). The related conditions most likely correspond to the upper flow regime, where the flow velocity of a stream v exceeds the wave's celerity c (Allen, 1997), i.e. the speed of a wave on the water surface. The ratio v/c between these velocities has been referred to as the Froude number F where $F>1$ denotes upper flow or supercritical conditions, while $F<1$ is characteristic for the lower flow regime or alternatively subcritical conditions (Engelund and Hansen, 1967). A hydraulic jump, which is characterized by a distinct increase in flow surface elevation and a decrease in flow velocity, then marks the downstream transition from a super- to a subcritical flow (Figure 1). Significant sediment accumulation may occur underneath the hydraulic jump upon deceleration of the flow's velocity (Slootman et al., 2018). Contrariwise, a downstream change from a lower to an upper flow regime occurs gradually and has no distinct surface expression, neither in terms of flow depth nor flow surface texture. While these mechanisms have been well explored and frequently reported both from modern environments and fine grained stratigraphic records (Alexander et al., 2001; Schlunegger et al., 2017; Slootman et al., 2018), less evidence for an upper flow regime has been documented from the coarse grained fraction of clastic sediments such as conglomerates. This even led Grant (1997) to note that upper flow regime conditions in fluvial channels are rare, and that the use of the Froude number for constraining flood and paleo-flood measurements lacks justifications from sedimentary records. In the same sense, Jarrett (1984) and Trieste (1992, 1994) considered that reports of inferred supercritical flows might be biased by underestimations of the bed roughness in mountainous streams. Nevertheless, because the entrainment of large clasts such as cobbles and boulders does involve large shear stresses and thus high discharge flows (Rust, 1978; Miall, 1978; Sinclair and Jaffey, 2001), it is possible that the transport and deposition of these particles, and particularly the formation of an imbricated fabric, is indeed related to changes in flow regimes (Figure 1). Here, we test this hypothesis for modern coarse-grained fluvial sediments and stratigraphic records. Similar to Grant (1997), we calculate the Froude number at conditions of incipient motion of coarse-grained bedload for various bed roughness and stream gradient values. We compare the results with data from modern streams and stratigraphic records and suggest that imbricated clasts are likely to provide evidence for supercritical flows, or at least for changes from upper to lower flow regimes over short distances (Figure 1).

Earth Surf. Dynam. Discuss., https://doi.org/10.5194/esurf-2018-35
Manuscript under review for journal Earth Surf. Dynam.
Discussion started: 3 May 2018

Methods

Expressions relating flow regime to channel gradient and bed roughness

Channel depth and grain size are the simplest and most straightforward variables that can be extracted from stratigraphic records (Duller et al., 2012). It has been shown that quantitative information about these variables can be used as basis to calculate paleo-slope and roughness values of streams for the geologic past (Paola and Mohring, 1996; Schlunegger and Norton, 2015). We therefore decided to focus on the simplest expressions relating channel depth and grain size to flow strength and sediment transport, such as that the resulting formulas can also be applied to sedimentological records. We are aware that this will be associated with large generalizations and simplifications, which will not consider the entire range of complexities that are usually associated with the transport of coarse-grained bedload in streams.

In the following, we consider the hydrological situation at the incipient motion of coarse-grained bedload. For these conditions, a dimensionless critical shear stress ϕ can be computed, which is the ratio between the fluid's shear stress τ_{cDx} and the particle's inertia force (Shields, 1936; Paola et al., 1992; Paola and Mohring, 1996; Tucker and Slingerland, 1997):

$$\phi = \frac{\tau_{cDx}}{(\rho_s - \rho) g D_x} \quad (1).$$

Here g is the gravity acceleration, ρ_s and ρ denote the sediment and water densities, respectively, and D_x is the grain size of interest. The relationship expressed in equation (1) predicts that a sediment particle with diameter D_x will be transported if the ratio between the fluid's shear stress τ_{cDx} and the particle's inertia force equals the value of ϕ. This dimensionless variable ϕ is also referred to as the Shields variable or the Shields stress. Assignments of values to ϕ vary considerably and range between c. 0.03 and 0.06, depending on the site-specific arrangement, the sorting, and the interlocking of the clasts (Buffington and Montgomery, 1997; Church, 1998). For instance, a channel floor made up of well-sorted material offers a greater resistance for the entrainment of embedded sediment particles than a gravel bar with a poorly sorted arrangement of the bed material. As a consequence, ϕ will be larger for well-sorted gravel bars than for poorly sorted ones. Mueller et al. (2005) also proposed that ϕ depends on channel gradients, where ϕ might exceed 0.1 for channels that are steeper than 1.1°. In either case, equation (1) can be transformed to an expression, which quantifies the critical shear stress for the entrainment of a sediment particle with a distinct grain size D_x:

$$\tau_{cDx} = \phi(\rho_s - \rho) g D_x \quad (2).$$

Among the various grain sizes, the D_{84} percentile has been considered as more suitable for the characterization of the gravel bar structure than the D_{50} (Howard, 1980; Hey and Thorne, 1986; Grant et al., 1990). In addition, the D_{84} has also been

Earth Surf. Dynam. Discuss., https://doi.org/10.5194/esurf-2018-35
Manuscript under review for journal Earth Surf. Dynam.
Discussion started: 3 May 2018

considered as a valuable parameter for the quantification of the relative bed roughness, which is defined as the ratio between grain size and water depth (e.g., Wiberg and Smith, 1991). If this inference is valid, then a major alteration of channel-bar arrangements requires a flow strength that is large enough to entrain the grain size represented by the 84th percentile. In this case, a Shields variable of ϕ=0.047 appears most appropriate (Meyer-Peter and Müller, 1948; Andrews, 1984). Therefore, the relationship of equation (2) for channel forming floods takes the form:

$$\tau_{cD_{84}} = 0.047 * (\rho_s - \rho) D_{84} \quad (3).$$

Bed shear stress is calculated using the approximation for an uniform flow down an inclined plane (e.g. Tucker & Slingerland, 1997), where:

$$\tau = g\rho S d \quad (4).$$

Here, *S* denotes the channel gradient, and *d* is the water depth. This relationship has been considered as adequate for streams where channel widths are more than 20 times larger than water depths, which is commonly the case for most rivers (Tucker and Slingerland, 1997).

Alternatively, bed shear stresses can also be computed as a function of the kinetic energy (Ferguson, 2007), where:

$$\tau = \frac{f}{8} \rho v^2 \quad (5).$$

In this relationship, *v* is the flow velocity. The variable *f*, referred to as the Darcy-Weissbach friction factor (e.g., Papaevangelou et al., 2010), denotes the energy loss due to friction within the roughness layer at the bottom of the flow. It also considers skin friction effects within the flow column (Ferguson, 2007). Within the flow boundary layer, energy loss appears to be lower for channel floors with well-sorted gravel bars than poorly sorted ones. The same is the case for the characteristic grain size D_x where larger grains exert a greater frictional resistance on the flow than smaller ones. These relationships illustrate that assignments of values to *f* are complicated and vary considerably. Ferguson (2007) reduced these complexities to a single expression (equation 6), where he considered roughness-layer (Krogstad and Antonia, 1999) and skin friction effects on the velocity of a water column at its surface. In the Ferguson (2007) relationship, *f* depends on water depths *d* relative to the grain size D_{84} and thus on the relative bed roughness:

$$\frac{f}{8} = \frac{\left(\frac{D_{84}}{d}\right)^2}{a_2^2} + \frac{\left(\frac{D_{84}}{d}\right)^{1/3}}{a_1^2} \quad (6).$$

Here, a_1 and a_2 are constants that vary between 7–8 and 1–4, respectively (Ferguson, 2007). A calibration of equation 6 by Ferguson (2007), where the D_{84} was employed as threshold grain size, returned values of 7.5 and 2.36 for a_1 and a_2, respectively, which we adapt in this paper. We additionally considered possible consequences of energy loss through assignments of different values to the Shields (1936) variable (see explanation of equation 1 above). We are aware that we could also employ the Manning's number *n* for the characterization of the channel's fabric (Whipple, 2004) and the relative bed roughness (Jarrett, 1984). Related expressions predict that the Manning's number *n* hinges on the channel gradient and water depth only and does not consider a dependency on the bed structure. We thus prefer to use Ferguson's (2007) approach (eq. 6), which explicitly includes the relative bed roughness.

As outlined in the introduction, the Froude number F can be approximated through the ratio between the flow velocity v and the celerity of a surface wave c. For shallow water conditions, which is commonly the case for rivers and streams, this relationship can be computed if the water depth d is known:

$$F = \frac{v}{c} = \frac{v}{\sqrt{gd}} \quad (7).$$

Combining equation 4, 5, and 7 yields then a simple expression where:

$$F = \sqrt{8\frac{S}{f}} \quad (8).$$

This expression states that the flow regime, expressed here by the Froude number F, depends on two partly non-related variables. In particular, for a given bed friction f, which depends on the bed roughness, upper flow regime conditions tend to establish for steep channels. Contrariwise, lower regime flows may occur in a steep environment where poorly sorted material exerts a large resistance on the flow, thereby reducing the flow velocity and hence the Froude number. Accordingly, for channel forming floods, where the entrainment of sediment particles can be expressed through the Shields (1936) variable ϕ, the dependency of F on the channel gradient S can be computed through the combination of equations 3, 4, 6 and 8, where

$$F = \sqrt{\frac{S}{\left(\frac{\rho S}{\phi(\rho_s - \rho)}\right)^2 * a_2^{-2} + \left(\frac{\rho S}{\phi(\rho_s - \rho)}\right)^{1/3} * a_1^{-2}}} \quad (9).$$

Alternatively, also during channel forming floods, an expression where the Froude number depends on the bed roughness D_{84}/d only can be achieved through the combination of equations 3, 4 and 8:

$$F = \sqrt{8 * \frac{\phi(\rho_s - \rho)}{\rho * f} * \frac{D_{84}}{d}} \quad (10).$$

We thus use equations 9 and 10 to calculate the Froude numbers at the incipient motion of the D_{84} grain sizes. We then compare these results with data from modern streams and stratigraphic records.

Collection of data from modern streams and stratigraphic records

We used observations about clast arrangements in gravelly streams in Switzerland. We paid special attention to the occurrence of clast imbrications, as we hypothesize that this fabric is likely to document alternating shifts in flow regimes (Figure 1) upon sedimentation and gravel bar migration. We selected those sites for which Litty and Schlunegger (2017) reported grain size data (Table 1), and we compared the observed fabric with the local gradient, which we calculated from topographic maps at scales 1:10'000 over a reach of c. 500 m.

The selected streams are all situated around the Central Alps (Figure 2), have various upstream drainage basins and different source rock lithologies (Spicher, 1980) and grain size distributions. At sites where grain size data has been collected, the ratio between the clasts' medium *b*- and longest *a*-axes are constant and range between 0.67 and 0.72 irrespective of the grain size distribution in these streams (Litty and Schlunegger, 2017). For these sites, we calculated the bed roughness D/d at the incipient motion of the D_{84}. Here, related water depths d are determined through the combination of equations (3) and (4), and using the channel gradient S at these sites.

We finally identified possible relationships between channel gradient, bed roughness, and the occurrence of clast imbrications from stratigraphic records. We focused on the Late Oligocene suite of alluvial megafan conglomerates (Rigi and Thun sections, Figure 2) deposited at the proximal border of the Swiss Molasse basin. For these conglomerates, Garefalakis and Schlunegger (2018) and Schlunegger and Norton (2015) collected data about the depth and gradient of paleo-channels, and information about the grain size distribution along c. 3000 to 3600 m-thick sections (Table 1). We returned to these sections and examined c. 50 sites for the occurrence of clast imbrications along the conglomerate suites.

Results

Calculation of flow regimes as a function of bed roughness and channel gradient

We calculated the Froude numbers F at the incipient motion of the D_{84} grain sizes and compared these results with observations from modern streams and stratigraphic records. We avoided to calculate the Froude numbers for slopes steeper than 1.4° because channels tend to adapt a step-pool geometry (Whipple, 2014), for which our simple calculations might no longer apply. We set the thresholds for critical flow conditions to a Froude number F=0.9, which is consistent with estimations for the formation of upper flow regime bedforms by Koster (1978). Calculations were initially carried out using a Shields variable of ϕ =0.047, which appears appropriate for D_{84} grain sizes. The results reveal that the Froude Number increases with steeper channels (Figure 3A) and reach the field of critical conditions for ~0.5° slopes. The values reach a maximum of nearly 1 where

Earth Surf. Dynam. Discuss., https://doi.org/10.5194/esurf-2018-35
Manuscript under review for journal Earth Surf. Dynam.
Discussion started: 3 May 2018

channel gradients are between ~0.8°–1°. Froude numbers then slightly decrease for channels steeper than 1° and finally reach a value of 0.9 for gradients >1.2°. In the case of greater thresholds for the incipient motion of clasts, which is expressed through a larger Shields (1936) variable of ϕ=0.06, flows adapt a supercritical flow for channels steeper than ~0.4°. For poorly sorted beds where the thresholds for the entrainment of the D_{84} are less (expressed here through a lower Shields (1936) variable of ϕ=0.03), streams remain in the lower flow regime.

The Froude number pattern is quite similar for increasing bed roughness (Figure 3B). For threshold conditions expressed through a Shields (1936) variable ϕ=0.047, the Froude numbers increase with higher relative bed roughness. Supercritical conditions are reached for a roughness of c. 0.1, after which the Froude numbers decrease with greater roughness. At larger threshold conditions for sediment entrainment, expressed through a Shields variable ϕ=0.06, upper flow regime conditions might prevail for bed surface roughness values between 0.06 and 0.5. Smaller and larger roughness will keep the flow in the lower regime. Contrariwise, the stream will not shift to the upper regime for gravel beds with poorly sorted clasts and thus for low threshold conditions for the entrainment of material (Shields variable ϕ=0.03). Note that the consideration of the full range of roughness-layer and skin friction effects, expressed through the coefficients a_1 and a_2 in equation (8), shifts the pattern of Froude values to lower and higher values. But this will not alter the general finding that upper flow regime conditions at the incipient motion of gravels might be expected for channel gradients S that are steeper than 0.5°±0.1°, and for a bed roughness D_{84}/d greater than ~0.06.

We also calculated the Froude numbers for a Shields variable of ϕ=0.1, because observations have shown that thresholds for the entrainment of sediment particles increase with steeper channels (Mueller et al., 2005). We additionally considered the case where the Shields (1936) variable depends on the channel gradient S through $\phi=2.81*S+0.021$ (Mueller et al., 2005). These relationships have been established using bed load rating curves, which are based on field surveys in mountainous streams in North America and England. We found that the flows shift to critical conditions for channels steeper than between 0.5° and 0.6° (slope dependent variable ϕ) and for a bed roughness >0.04 (ϕ=0.1).

In summary, the calculations predict that water flow may shift to upper flow regime conditions for streams where channel gradients are steeper than ~0.5°±0.1°, and where relative bed roughness exceeds a value of ~0.06±0.01.

Data from modern streams

Grain size, channel morphology and stream runoff data are available for several streams in the northern, the central and the southern Swiss Alps. These rivers are situated both in the

Earth Surf. Dynam. Discuss., https://doi.org/10.5194/esurf-2018-35
Manuscript under review for journal Earth Surf. Dynam.
Discussion started: 3 May 2018

core of the Alps and the foreland. As mentioned above, the bedrock-geology of their headwaters includes the entire range of lithologies from sedimentary units to schists, gneisses and granites. In the same sense, the streams cover the full range of water sources in their headwaters including glaciers and surface runoff. Except for the Maggia River between the sites Bignasco and Losone (Figure 2), all streams are channelized, and the rivers generally flow in a bed that is laterally confined by artificial riverbanks. These are either made up of concrete walls or outsized boulders. The thalweg of the streams then meanders between these walls within a 20 to 50 m-wide belt. Flat-topped longitudinal bars that are several tens of meters long and that emerge up to 1.5 m above the thalweg are situated adjacent to the artificial riverbanks on the slip-off slope of these meanders. They evolve into transverse bars, or riffles, farther downstream where the thalweg shifts to the opposite channel margin. Channels are deepest and flattest along the outer cutbank side of the meanders and in pools downstream of riffles, respectively. The thalweg then steepens where it crosses the transverse bars and riffles. This is also the location where the stream shows evidence for standing waves (e.g., at Reuss, Figures 2, 4A). Standing waves have also been encountered at Waldemme Littau (Figures 2, 4B) when water runoff at that particular site was c. 100 m^3/s and when rumbling sounds suggested that clasts were rolling or sliding. The streams thus display a complex pattern where channel depths, flow velocities and possibly also hydrological regimes alternate over short distances of tens to hundreds of meters. These arrangements of channel-bar pairs and their positions within the channel belt has been stable over the past years as the locations of the gravel bars are still the same as the ones reported by Litty and Schlunegger (2016).

Inspections of gravel bars have shown clear evidence for imbrications in the Glenner, the Landquart, the Verzasca, and the Waldemme rivers (Table 1). In these streams, channel gradients range between 0.6° (Waldemme) and 1.2° (Glenner) (Figure 3C). In addition, the sizes of the D_{84} range between 3 cm (Waldemme) and 12 cm (Glenner). The gravel lithology includes the entire variety from sedimentary (Waldemme) to crystalline constituents (Glenner, Landquart, Verzasca). The inferred bed roughness at the incipient motion of the D_{84} includes the range between c. 0.125 (Waldemme) and 0.31 (Glenner) (Figure 3D).

At Maggia, Reuss and Waldemme Littau, the largest clasts are arranged as triplets or quadruplets of imbricated constituents within generally flat lying to randomly-oriented finer grained sediment particles. The density of these arrangements ranges between 5 groups per 10 m^2 (Maggia Bignasco, Maggia Losone) to c. 10 groups per 10 m^2 (Maggia Visletto, Reuss, Waldemme Littau e.g. Figure 4D). The channel gradients at these sites span the range between c. 0.3 and 0.6°, and the D_{84} clasts are between 3 and 9 cm large (Reuss and Maggia Visletto). Accordingly, the relative bed roughness at the incipient motion of the D_{84} ranges between 0.07 and 0.16.

Gravel bars within the Emme and Sense (Figure 4C) streams are made up of generally flat lying gravels and cobbles. This is particularly the case in pools and on the upstream stoss-side of longitudinal and transverse bars where channel gradients are flat (Table 1; Figures 3C, 3D). In both streams, clast imbrications occur in places only where gravel bars have steep downstream slip faces, which are mainly observed at the end of transverse bars. Also in these streams, channel gradients are less than 0.5°. The sizes of the D_{84} measure between 2 cm (Emme) and 6 cm (Sense). The bed roughness of these streams, calculated for the incipient of motion of the 84th grain size percentile, ranges between 0.07 and 0.10.

Data from stratigraphic records

We used published data about channel depth d, surface gradients S and information about the pattern of the D_{84}, which have been reported from the Late Oligocene alluvial megafan conglomerates at Rigi (47°03'N / 8°29'E) and Thun (46°46'N / 7°44'E) situated in the Molasse foreland basin north of the Alpine orogen (Table 1). The depositional evolution of these conglomerates has been related to the rise of the Alpine mountain belt and the associated erosional history of this orogen (Kempf et al., 1999; Schlunegger and Castelltort, 2016). We calculated patterns of bed roughness and related channel gradients and explored c. 50 conglomerate sites for the occurrence or absence of clast imbrications.

The deposits at Rigi are c. 3600 m thick and made up of an alternation of conglomerates and mudstones (Stürm, 1973) that were deposited between 30 and 25 Ma according to magneto-polarity chronologies and mammal biostratigraphic data (Engesser and Kälin, 2017). Garefalakis and Schlunegger (2018) subdivided this alternation of conglomerates and mudstones into four segments labeled as α through δ. The lowermost segments α and β are an alternation of mudstones and conglomerate beds and were deposited by gravelly streams where channels were laterally bordered, and thus confined, by a floodplain (Stürm, 1973). According to Garefalakis and Schlunegger (2018), the depositional area was characterized by a low surface slope ranging between 0.2±0.06° and 0.4±0.2°. Channel depths span the range between 1.7 and 2.5 m, and the D_{84} values are between 2 and 6 cm. These measurements result in bed roughness values between 0.02 and 0.05. We found no imbrications at 13 sites (Figures 3C, 3D, 4E), and only one conglomerate outcrop displayed evidence for clast imbrications.

The top of the Rigi section, referred to as segments γ and δ by Garefalakis and Schlunegger (2018), is an amalgamated stack of conglomerate beds deposited by non-confined braided streams (Stürm, 1973). Garefalakis and Schlunegger (2018) inferred values between 0.65±0.2° and 0.9±0.4° for the paleo-gradient of these rivers (Table 1). D_{84} values range between 6 and 12 cm, and paleo-channels were c. 1.2 m deep. This yields a relative bed roughness between c. 0.05 and 0.12. Interestingly, a large number of conglomerate sites within the segments γ and δ display evidence for clast imbrications

(Figures 3D, 4F). However, at all sites, the lateral extents of groups with imbricated clasts are limited to widths of 1-2 meters.

The up to 3000 m-thick conglomerates at Thun are slightly younger, and the ages span the time interval between c. 26 and 24 Ma according to magneto-polarity chronologies (Schlunegger et al., 1996). Similar to the Rigi section, the conglomerates at Thun start with an alternation of conglomerates, mudstones and sandstones, which has been referred to as unit A. This suite is overlain by an up to 2000 m-thick amalgamated stack of conglomerate beds (unit B). Channel depths within unit A range between 3 to 5 m, and streams were between 0.1° and 0.3° steep. Channels in the overlying unit B were shallower and between 1.5 and 3 m deep. Stream gradients varied between 0.4° and 1°, depending on the relationships between inferred water depths and maximum clast sizes (Schlunegger and Norton, 2015). In this section, sequences with imbricated clasts have only been found in unit B where paleo-channel slopes were steeper than 0.4° (Figure 3C). Similar to the Rigi section, the lateral extents of groups with imbricated clasts are limited to widths of a few meters only. No data is available for computing the D_{84} grain size, with the consequence that we cannot estimate the bed roughness for the Thun conglomerates.

Discussion

Relationships between channel gradient, bed roughness and flow regime

We have found an expression where the Froude number *F*, and thus the change from the lower to the upper flow regime, depends on the channel gradient *S* and the bed roughness *D/d* (eq. 8). This relationship also predicts that the controls of both parameters on the Froude number are to some extent independent from each other. Under these considerations, the similar pattern of how the Froude number *F* depends on channel gradient and bed roughness (Figures 3A and 3B) appears unexpected. However, we note that we computed both relationships for the case of the incipient motion of the grain size percentile D_{84}. This threshold is explicitly considered by equation 3, which we used as basis to derive an expression where the Froude number depends on the channel gradient or the bed roughness only. Therefore, it is not surprising that the dependencies of the Froude number on gradient and bed roughness follow the same trends. In addition, Blissenbach (1952), Paola and Mohring (1996) and also Church (2006) showed that channel gradient, water depth and grain size are closely related parameters during channel forming floods. In particular, channels with coarser grained gravel bars tend to be steeper and shallower than those where the bed material is finer grained (Church, 2006). In the same sense, also in steeper streams, bed roughness values tend to be larger than in flatter channels (Whipple, 2004). We use the causal relationships between these variables to explain the similarity in the patterns illustrated in Figures 3A and 3B.

The tendency towards lower Froude numbers for a channel gradient >1° (ϕ >0.047) and a bed roughness >0.3 (ϕ >0.047) is somewhat unexpected. We explain these trends through the relationships denoted in equation 1, which states that shallower floods (lower *d*) require steeper channels for the entrainment of the D_{84} clasts. The result is a lower surface velocity relative to the same bottom shear stress of a flow. This is the case because the energy loss within the roughness-layer has a relatively large effect on the velocity at the flow's surface if the water column is shallow. The same relationships are expected for a large bed roughness.

Relationships between flow regimes and clast imbrications

Here, we provide evidence for linking the occurrence of clast imbrications with shifts from supercritical to subcritical flows. However, interpretations of the linkages between hydrological conditions upon transport and the fabric of gravel bars are hampered because related flume experiments are not available. Nevertheless, for the North Saskatchewan River in Canada, Shaw and Kellerhals (1977) reported gravel mounds on a lateral gravel bar, which have a regular spacing between 2 and 3 m and a relatively flat top. Shaw and Kellerhals considered these bedforms as antidunes, which might have formed in the upper flow regime. Also in modern gravelly streams, transverse ribs, which are a series of narrow, current-normally orientated accumulations of large clasts, were considered as evidence for the deposition either under upper flow regime conditions, or in response to upstream-migrating hydraulic jumps (e.g., Koster, 1978; Rust and Gostin, 1981). Koster (1978) additionally reported that these bedforms are associated with clast imbrications (Figure 2 in Koster, 1978). Alexander and Fielding (1997) found modern gravel antidunes with well-developed clast imbrications in the Burdekin River, Australia. Finally, Taki and Parker (2005) reported cyclic steps of channel floor bedforms with wave-lengths that are 100–500 times larger than the flow thickness. These bedforms most likely represent chute-and-pool configurations (Taki and Parker, 2005), which could have formed in response to alternations of upper and lower flow regime conditions, as outlined by Grant (1997). In such a situation, the upstream flow on the stoss-side of the bedform may experience a reduction of the flow velocity, with the effect that the flow may shift to subcritical conditions. This is associated with a hydraulic jump and a drastic reduction of the flow velocity and thus a drop in shear stresses (Figure 1). In gravelly streams, such a situation most likely results in the deposition of clasts. We use these mechanisms to explain the formation of clast imbrications, which record an upstream migration of the site where sediment accumulates (Figure 5). Accordingly, the occurrence of clast imbrications might record alternating shifts from upper to lower flow regimes separated by hydraulic jumps, which will also migrate upstream as the construction of the imbricated fabric proceeds (Figure 5). We support this interpretation through our generic calculations (Figures 3A, 3B) in combination with observations from modern streams in the Central European Alps (Figure 3C) and from stratigraphic records (Figure 3D). For both observational datasets, we find gravel bars with imbricated clasts in streams with a bed roughness >0.06 and a slope >0.5°, consistent with

Earth Surf. Dynam. Discuss., https://doi.org/10.5194/esurf-2018-35
Manuscript under review for journal Earth Surf. Dynam.
Discussion started: 3 May 2018

the theoretical predictions for the occurrence of upper flow regime conditions (Figure 3). This threshold slope is also supported by the results of previous work, where upper flow regime bedforms such as transvers ribs have been described for e.g., the Peyto Outwash (slope c. 1.09°), the Spring Creek (same slope; McDonald and Banerjee, 1971), and the North Saskatchewan River (slope 0.52°; Dept. Mines and Tech. Survs., 1957). However, Simons and Richardson (1960, p. 45) noted that flows rarely exceeded unity Froude numbers over an extended period of time in a stream with erodible banks. We thus use the conclusion of their discussion to explain the limited spatial extent of individual ensembles of imbricated clasts in modern streams and stratigraphic records.

Relationships between channel gradients, flow strengths and imbrication of clasts

Steeper slopes result in stronger flow strengths and faster flow velocities, which in turn are required to exceed the larger thresholds exerted by imbricated clasts. This is the major conclusion of the following paragraph, where we link the arrangement of clasts to thresholds of flow strengths through force balancing. In this context, it has been shown (Li and Komar, 1986) that the transport of coarse-grained bedload material can either be accomplished through sliding and/or rolling (Figure 6A). Sliding of clasts maintain the sediment particles in a flat position where *a*-*b*-planes are lying parallel to the channel floor, as exemplified by a large number of gravel bars in the Sense stream (Figure 4C). In contrast, the occurrence of clast imbrications requires that some of the clasts were transported through rolling (Figure 5A). In both cases, the forces operating on a sediment particle through the ambient fluid can best be described as the combined effect of a lift and a drag component (Shields, 1936; Allen, 1997). An individual grain then begins to move if the resulting fluid force F_{fluid} exceeds the submerged weight F_g of the sediment particle with grain size D. In the case of rolling, the rotation of a clast occurs if the moment exerted by the fluid's force F_{fluid} exceeds the moment due to the clast's inertia force (e.g., Shields, 1936; Allen, 1997), where:

$$D * F_{fluid} * \sin(\alpha) \geq \frac{D}{2} * F_g * \cos(\alpha - \beta) \quad (11).$$

Here, D denotes the grain size and corresponds to the length of the clast's medium b-axis. Note that we employed the grain size D as measure for the torsion arm for simplification purposes. α represents the angle of repose or the pivoting angle of the clast, and β denotes the direction of the fluid force relative to the channel bed. At the incipient motion through rolling or pivoting (Komar, 1996, p 165 ff), the ratio between shear and inertia forces corresponds to the following relationships:

$$\frac{F_{fluid}}{F_g} = 0.5 * \frac{\sin(\alpha)}{\cos(\alpha - \beta)} < 0.5 * \sin(\alpha) \quad (12).$$

Accordingly, the strength F_{fluid} required for the initiation of movement strongly depends on the size and the position of the clast with respect to F_{fluid}, expressed here through the pivoting angle α. Equation (12) predicts that at the incipient motion of a grain, the ratio in equation (12) becomes larger than the Shields variable ϕ for α >5–10°, and even one magnitude greater if the clast pivots around an angle >35°, which has been considered as a common dip angle of imbrication (e.g., Shao et al., 2014).
Through experiments conducted on up to 3 cm-large grains, Shields (1936) and then also Meyer-Peter and Müller (1948) reported that at the incipient motion of the grains, the ratio between the fluid force and the clast's inertia force F_{luid}/F_g ranges between c. 0.03 and 0.06. According to Meyer-Peter and Müller (1948), this ratio is quite robust and does not depend on whether the grains roll or slide on the substratum. These experiments, however, were conducted with spherical grains only and did not include oblate particles. In 1986, Li and Komar performed flume experiments with both oblate and spherical sand- and gravel-sized grains. They showed that oblate clasts preferentially tend to slide out of position. In the same experiments, pivoting around small angles of a few degrees occurred only if the grains had nearly circular cross-sections (Li and Komar, 1986). This suggests that for oblate clasts, a displacement through sliding requires a lower fluid force than through pivoting and rolling. The experiments by Li and Komar (1986) thus imply that the formation of clast imbrications is associated with relatively large fluid forces, and thus large shear stresses and large flow velocities, which in turn are promoted through steeper slopes. As a further implication of these relationships, the Shields (1936) variable ϕ, which denotes the ratio between the critical shear stress τ_c and the clast's inertia force F_g at the incipient motion of a sediment particle, should be larger for steeper slopes. This is consistent with observations (Mueller et al., 2005) and the results of theoretical work (Lamb et al., 2008). In particular, Mueller et al. (2005) suggested that a ϕ value of c. 0.03 is suitable for slopes <0.35°, while ϕ > 0.1 might be more appropriate for the mobilization of coarse-grained sediment particles in channels steeper than 1.1°.

Summary and conclusions

We started with the hypothesis that the transport and deposition of coarse-grained particles, and particularly the formation of an imbricated fabric, is related to changes in flow regimes. We then calculated the Froude number F at conditions of incipient motion of coarse-grained bedload for various bed roughness and stream gradient values, and we compared the results with data from modern streams and stratigraphic records. The results suggest that imbricated clasts are likely to provide evidence for the occurrence of supercritical conditions, or at least for changes from upper to lower flow regimes particularly at sites where channel gradients are steeper than ~0.5°. We do acknowledge that our field-based inferences are associated with large uncertainties regarding channel gradients and grain size (Litty and Schlunegger, 2017), and that they lack a quantitative measure of the spatial distribution of clast imbrications and clast arrangements. In the same sense, the hydrologic calculations and force balancing approaches are based on the simplest published expressions where water flow is related to sediment transport. Larger complexities, which complicate any considerations of material transport (Engelund and Hansen, 1967), have not been taken considered. This includes, for instance, large supply rates of sediment (Bekaddour et al., 2013), changes in bed morphology, spatial variations in turbulences, the shape and the sorting of grains, and the 3D arrangement of clasts (Lamb et al., 2008). Despite our simplifications, we do find evidence for relating the occurrence of clast imbrications to upper flow regime conditions. In particular, an imbricated arrangement of clasts forms through rolling, or pivoting, and when the clasts come to a rest behind a larger sediment particle. For an oblate grain, thresholds for pivoting are larger than for sliding, with the consequence that larger fluid forces are required to mobilize the bedload upon rolling. Greater fluid forces can be accomplished through larger flow velocities, with the result that the flows become supercritical. We propose that this is likely to occur, when channel gradients become steeper than c. 0.5°±0.1° and when bed roughness also gets larger. We thus conclude that clast imbrications do record the occurrence of supercritical flows and may be associated with alternating shifts in flow regimes paired with hydraulic jumps. These findings might be useful for the quantification of hydrological conditions in coarse-grained stratigraphic archives such as conglomerates. As a further implication, the occurrence of imbrications in clastic sediments may be used to infer a minimum value of 0.5°±0.1° for the paleo-topographic slope. Such a constraint might be beneficial for paleo-geographic reconstructions and for the analysis of a basin's subsidence history through the back-stripping of strata (e.g., Schlunegger et al., 1997). Finally, for modern streams, the presence of clast imbrications might be more conclusive for inferring an upper flow regime upon material transport than other bedforms such as transverse ribs or antidunes (Koster, 1978; Rust and Gostin, 1981), mainly because clast imbrications have a better preservation potential and are easier to recognize in the field.

Figure captions

Figure 1: A) Photo showing hydraulic jump. B) Conceptualization of situation displayed in photo of Figure 1A. *F*=Froude number; *v*=flow velocity, *d*=water depth.

Figure 2: Sites where modern gravel bars in streams were inspected for the occurrence of clast imbrications. The figure also shows the locations of the stratigraphic sections where conglomerates were analyzed for their sedimentary structures. *S*=Sense; *E*=Emme; $WE_{I\text{-}IV}$=Waldemme, *WL*=Waldemme at Littau, *R*=Reuss;

L=Landquart; *G*=Glenner; M_B, M_V, M_L=Maggia at Bignasco, Visletto and Losone; V_F, V_M, V_L=Verzasca at Frasco, Motta and Lavertezzo. See Table 1 for coordinates of sites.

Figure 3: Relationships between A) channel slope and Froude number *F*, and B) relative bed roughness and *F*. These were calculated as a function of various Shields (1936) variables ϕ. The pale blue field indicates the conditions where an upper flow regime could prevail, while the red field delineates the occurrence of lower flow regime conditions. In this context, we set the threshold to a Froude number of c. 0.9. This is consistent with the estimation of parameters for the formation of upper flow regime bedforms by Koster (1978). The lower figures relate the occurrence of imbrications (blue bars) or no imbrications (red bars) to channel slopes C) and to relative bed roughness D). Red bars with blue hatches indicate that imbrications have been found in places. Blue bars with red hatches suggest that imbrications dominate the bar morphology, but that reaches without imbrications are also present on the same gravel bar. Data from modern streams are displayed above the horizontal axes, while information from stratigraphic sections are placed below the slope and roughness axes, respectively. *S*=Sense, *E*=Emme, WE_{I-IV}=Waldemme, *WL*=Waldemme at Littau, *R*=Reuss; *L*=Landquart; *G*=Glenner; M_B, M_V, M_L=Maggia at Bignasco, Visletto and Losone; V_F, V_M, V_L=Verzasca at Frasco, Motta and Lavertezzo. See Table 1 for coordinates of sites, and Figure 2 for locations where data were collected.

Figure 4: Photos from the field. A) Transverse and lateral bars in the Reuss River with imbricated clasts on the lateral bar forming a riffle, and standing waves where the thalweg crosses the riffle. Arrow indicates flow direction. B) Standing waves with a wavelength of c. 8 m in the Waldemme at Littau. Water fluxes are c. 100 m^3/s. Arrow indicates flow direction. C) Flat lying clasts on a lateral bar in the Sense River. D) Imbricated clasts within the Maggia River at Visletto. Arrow indicates flow direction. E) Conglomerates at Rigi with no evidence for clast imbrications. White lines indicate the orientation of the bedding. F) Conglomerates at Rigi with imbricated gravels to cobbles. Arrow indicates paleoflow direction. White line refers to the bedding. See Figure 2 for location and Table 1 for coordinates.

Figure 5: Conceptual sketch illustrating the formation of an ensemble of imbricated clasts as time proceedes (A through C). The formation of such a sedimentary fabric requires that clasts are transported upon rolling. A hydraulic jump forms

at the upstream end of the suite of imbricated clasts, because the flow on the stoss-side of the bedform most likely experiences a reduction of the flow velocity. This can then result in aggradation of clasts due to the drop of the shear stress. According to this model, the site of sediment accumulation will migrate upstream. *F*=Froude number; *v*=flow velocity, *d*=water depth.

Figure 6: A) Illustration of possible transport mechanisms of coarse grained bedload. The mobilization can be accomplished through sliding or rolling. Modified after Allen (1997). B) Forces operating on a clast upon sliding, and C) force balancing of a clast upon pivoting. See text for further information.

Table 1: Data that has been collected in the field. See text for further explanations.

Author contribution

FS designed the study and carried out the calculations, PG and FS collected the data, FS wrote the text with contributions by PG, both authors contributed to the analyses and discussion of the results.

Data availability

All data used in this publication are available.

Data availability

The authors declare they have no conflict of interest.

Acknowledgements

This research has been supported grant No 154198 awarded to Schlunegger by the Swiss National Science Foundation.

References

Allen, P.A., Earth Surface Processes, John Wiley and Sons, Oxford, 416 pp., 1997.

Andrews, E.D., Bed-material entrainment and hydraulic geometry of gravel-bed rivers in Colorado, GSA Bull., 95, 371-378, 1984.

Alexander, J., Bridge, J.S., Cheel, R.J., and Leclair, S.F., Bedforms and associated sedimentary structures formed under supercritical water flows over aggrading sand beds, Sedimentology, 48, 133-152, 2001.

Alexander, J., and Fielding, C., Gravel antidunes in the tropical Burdekin River, Queensland, Australia, Sedimentology, 44, 327-337, 1997.

Blissenbach, L., Relation of surface angle distribution to particle size distribution on alluvial fans, J. Sediment. Petrol., 22, 25–28, 1952.

Bekaddour, T., Schlunegger, F., Attal, M., and Norton, P.K., Lateral sediment sources and knickzones as controls on spatio-temporal variations of sediment transport in an Alpine river, Sedimentology, 60, 342-357, 2013.

Buffington, J.M., and Montgomery, D. R., A systematic analysis of eight decades of incipient motion studies, with special reference to gravel-bedded rivers, Water Resour. Res., 33, 1993-2029, 1997.

D'Arcy, M., Roda-Boluda, D.C., and Whittaker, A.C., Glacial-interglacial climate changes recorded by debris flow fan deposits, Owens Valley, California, Quat. Sci. Rev., 169, 288-311, 2017.

Church, M., Palaeohydrological reconstructions from a Holocene valley fill, Fluvial sedimentology, edited by: Miall, A.D., Mem. Can. Soc. Petrol. Geol., 5, 743-772, 1978.

Church, M., Bed material transport and the morphology of alluvial river channels, Ann. Rev. Earth Planet. Sci., 34, 325–354, 2006.

Department of Miines and Technology Surveys, Atlas of Canada, Geogr. Branch, Ottawa, 1957.

Duller, R.A., Whittaker, A.C., Swinehart, J.B., Armitage, J.J., Sinclair, H.D., Bair, A., and Allen, P.A., Abrupt landscape change post-6Ma on the central Great Plains, USA, Geology, 40, 871-874, 2012.

Engesser, B., and Kälin, D., *Eomys helveticus* n. sp. and *Eomys schluneggeri* n. sp., two new small eomyids of the Chattian (MP 25/MP 26) subalpine Lower Freshwater Molasse of Switzerland, Fossil Imprint, 73, 213–224, 2017.

Engelund, F., and Hansen, E., A monograph on sediment transport in alluvial streams, Teknisk Forlag – Copenhagen, 62 pp., 1967.

Ferguson, R., Flow resistance equations for gravel- and boulder- bed streams. Water Resour. Res., 43, W05427, 2007.

Garefalakis, P., and Schlunegger, F., Link between concentrations of sediment flux and deep crustal processes beneath the European Alps, Sci. Rep., 8, 183, doi:10.1038/s41598-017-17182-8

Grant, G.E., Swanson, F.J., and Wolman, M.G., Pattern and origin of stepped-bed morphology in high gradient streams, western Cascades, Oregon, GSA Bull., 102, 340–352, 1990.

Grant, G.E., Critical flow constrains flow hydraulics in mobile-bed streams: A new hypothesis, Water Resour. Res, 33, 349-358, 1997.

Hey, R.D., and Thorne, C.R., Stable channels with mobile gravel beds, J. Hydr. Eng., 112, 671-689, 1986.

Howard, A.D., in: Thresholds in Geomorphology, edited by: Coates, D.R., and Vitek, J.D., Allen and Unwin, Boston, MA, 227-258, 1980.

Jarrett, R.D., Hydraulics of high-gradient streams. J. Hydr. Eng., 110, 1519-1939, 1984.

Kempf, O., Matter, A., Burbank, D.W., and Mange, M., Depositional and structural evolution of a foreland basin margin in a magnetostratigraphic framework; the eastern Swiss Molasse Basin, Int. J. Earth Sci., 88, 253–275, 1999.

Komar, P.D., Entrainment of sediments from deposits of mixed grain sizes and densities, in: advances in fluvial dynamics and stratigraphy, edited by Carling, P.A., and Dawson, M.R., John Wiley and Sons, Chichester, 127-181, 1996.

Koster, E.H., Transverse ribs: their characteristics, origin and paleohydrauic significance, in: Fluvial sedimentology, edited by: Miall, A.D., Mem. Can. Soc. Petrol. Geol., 5, 161-186, 1978.

Krogstad, P.A., and Antonia, R.A., Surface roughness effects in turbulent boundary layers, Exp. Fluids, 27, 450-460, 1999.

Lamb, M.P., Dietrich, W.E., and Venditti, J.G., Ist he critical Shields stress for incipient sediment motion dependent on channel bed slope?, J. Geophys. Res., 113, F02008, 2008.

Li, Z., and Komar, P.D., Laboratory measurements of pivoting angles for applications to selective entrainment of gravel in a current, Sedimentology, 33, 413-423, 1986.

Litty, C., and Schlunegger, F., Controls on pebbles' size and shapes in streams oft he Swiss Alps, J. Geol., 123, 405-427, 2017.

Matter, A.: Sedimentologische Untersuchungen im östlichen Napfgebiet (Entlebuch – Tal der Grossen Fontanne, Kt. Luzern), Eclogae Geol. Helv., 57, 315-428, 1964.

McDonald, B.C., and Banerjee, I., Sediments and bedforms on a braided outwash plain, Can. J. Earth Sci., 8, 1282-1301, 1971.

Meyer-Peter, E., and Müller, R., Formulas for bedload transport, Proceedings of the 2nd meeting of the Int. Assoc. Hydraul. Struct. Res., Stockholm, Sweden. Appendix 2, 39–64, 1948.

Miall, A.D., Fluvial sedimentology: An historical overview, in: Fluvial sedimentology, edited by: Miall, A.D., Mem. Can. Soc. Petrol. Geol., 5, 1-48, 1978.

Middleton, L.T., and Trujillo, A.P., Sedimentology and depositional setting of the upper Proterozoic Scanlan Conglomerate, central Arizone. In: Sedimentology of gravels and conglomerates, edited by: Koster, E.H., and Steel, R.J., Mem. Can. Soc. Petrol. Geol., 10, 189-202, 1984.

Mueller, E.R., Pitlick, J., and Nelson, J.M., Variation in the reference Shields stress for bed load transport in gravel-bed streams and rivers, Water Resour. Res., 41, W04006, 2005.

Papaevangelou, G., Evangelides, C., and Tsimopoulos, C., A new explicit relation for friction coefficient f in the Darcy-Weisbach equation, Proc. 10th Conf. Prot. Restor. Env., PRE10, July 6-9, 2010.

Paola, C., Heller, P.L., and Angevine, C., The large-scale dynamics of grain-size variation in alluvial basins, 1: Theory, Basin Res., 4, 73-90, 1992.

Paola, C, and Mohring, D., Palaeohydraulics revisted: palaeoslope estimation in coarse-grained braided rivers. Basin Res., 8, 243-254, 1996.

Pettijohn, F.J., Sedimentary rocks, Harper and Brothers, New York, 718 pp., 1957.

Potsma, G., and Roep, T., Resedimented conglomerates in the bottomsets of Gilbert-type gravel deltas, J. Sed. Petrol., 55, 874-885, 1985.

Rust, B.R., Depositional models for braided alluvium, in: Fluvial sedimentology, edited by: Miall, A.D., Mem. Can. Soc. Petrol. Geol., 5, 221-245, 1978.

Rust, B.R., Proximal braidplain deposits in the Middle Devonian Malbaie Formaiton of eastern Gaspé, Quebec, Canada, Sedimentology, 31, 675-695, 1984.

Rust, B.R., and Gostin, V.A., Fossil transverse ribs in Holocene alluvial fan deposits, Depot Creek, South Australia, J. Sediment. Petrol., 51, 441-444, 1981.

Shao, Z., Zhong, J., Li, Y., Mao, C., Liu, S., Ni, L., Tian, Y., Cui, X., Liu, Y., Wang, X., Li, W., and Lin, G., Characteristics and sedimentary processes of lamina-controlled sand-particle imbricate structure in deposits of Lingshan Island, Qingdao, China, Sci. China Earth Sci., 57, 1061-1076, 2014.

Schlunegger, F., Burbank, D.W., Matter, A., Engesser, B., and Mödden, C., Magnetostratigraphic calibration of the Oligocene to Middle Miocene (30-15 Ma) mammal bizones and depositional sequences of the central Swiss Molasse basin, Eclogae geol. Helv., 89, 753-788, 1996.

Schlunegger, F., Jordan, T.E., and Klaper, E.M., Controls of erosional denudation in the orogeny on foreland basin evolution: The Oligocene central Swiss Molasse Basin as an example, Tectonics, 16, 823-840, 1997.

Schlunegger, F., and Norton, K.P., Climate vs. tectonics: the competing roles of Late Oligocene warming and Alpine orogenesis in constructing alluvial megafan sequences in the North Alpine foreland basin, Basin Res., 27, 230-245, 2015.

Schlunegger, F., Norton, K.P., Delunel, R., Ehlers, T.A., and Madella, A., Late Miocene increase in precipitation in the Western Cordillera of the Andes between 18-19° latitudes inferred from shifts in sedimentation patterns, Earth Planet. Sci. Lett., 462, 157-168, 2017.

Schlunegger, F. and Castelltort, S., Immediate and delayed signal of slab breakoff in Oligo/Micoene Molasse deposits from the European Alps, Sci. Rep. 6, 31010, 2016.

Shaw, J, and Kellerhals, R., Paleohydraulic interpretation of antidune bedforms with applications to antidunes in gravel, J. Sediment. Petrol., 47, 257-266, 1977.

Shields, A., Andwendungen der Aehnlichkeitsmechanik und der Turbulenzforschung auf die Geschiebebewegung. Mitt. Preuss. Versuch. Wasserbau Schiffbau, 26, Berlin, 1936.

Simons, E.V., and Richardson, E.V., Discussion of resistance properties of sediment-laden streams, Am. Soc. Civil Eng. Trans., 125, 1170-1172, 1960.

Sinclair, H.D., and Jaffey, N., Sedimentology of the Indus Group, Ladakh, northern India: implications for the timing of initiation of the paaeo-Indus River. J. Geol. Soc. London, 158, 151-162, 2001.

Slootman, A., Simpson, G., Castelltort, S., and De Boer, P.L., Geological record of marine tsunami backwash: The role of the hydraulic jump, Depositional Record, 1-19, 2018.

Spicher, A., Geologische Karte der Schweiz 1:500'000, Schweiz. Natf. Ges., 1980.

Stürm, B., Die Rigischüttung. Sedimentpetrographie, Sedimen tologie, Paläogeographie, Tektonik, PhD thesis, Univ. Zürich, Switzerland, 98 p., 1973.

Taki, K., and Parker, G., Transportational cyclic steps cre- ated by flow over an erodible bed. Part 1. Experiments, J. Hydrol. Res., 43, 488–501, 2005.

Todd, S.P., Process deduction from fluvial sedimentary structures, in: Advances in fluvial dynamics and stratigraphy, edited by: Carling, P.A., and Dawson, M.R., John Wiley & Sons Ltd, 299-350, 1996.

Trieste, D.J., Evaluation of supercritical/subcritical flows in high-gradient channel, J. Hydr. Eng., 118, 1107-1118, 1992.

Trieste, D.J., Supercritical flows versus subcritical flows in natural channels, in: Hydraulic Engineering '94: Proceedings of the 1994 Conference of the Hydraulics Division, edited by: Cotroneo, G.V., and Rumer, R.R., Am. Soc. Civ. Eng., New York, 732-736, 1994.

Tucker, G., and Slingerland, R., Drainage basin responses to climate change, Water Resour. Res., 33, 2031-2047, 1997.

Whipple, K.X., Bedrock rivers and the geomorphology of active orogens, Ann. Rev. Earth Planet. Sci., 32, 151–185, 2004.

Wiberg, P.L., and Smith, J.D., Velocity distribution and bed roughness in high-gradient streams, Water Resour. Res., 27, 825-838, 1991.

Yagishita, K., Paleocurrent and fabric analyses of fluvial conglomerates of the Paeogene Noda Group, northeast Japan, Sed. Geol., 109, 53-71, 1997.

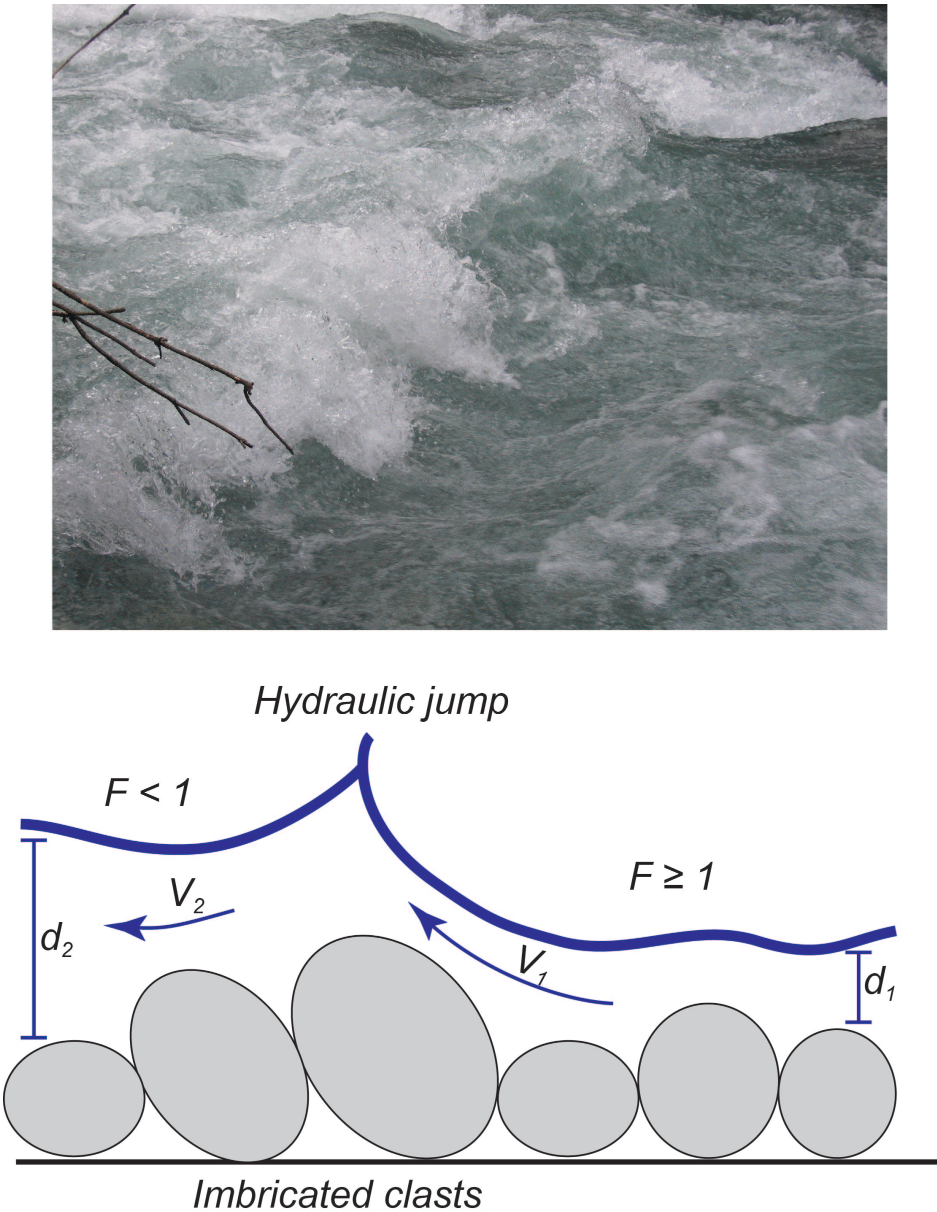

A

B

Figure 1

Earth Surf. Dynam. Discuss., https://doi.org/10.5194/esurf-2018-35
Manuscript under review for journal Earth Surf. Dynam.
Discussion started: 3 May 2018

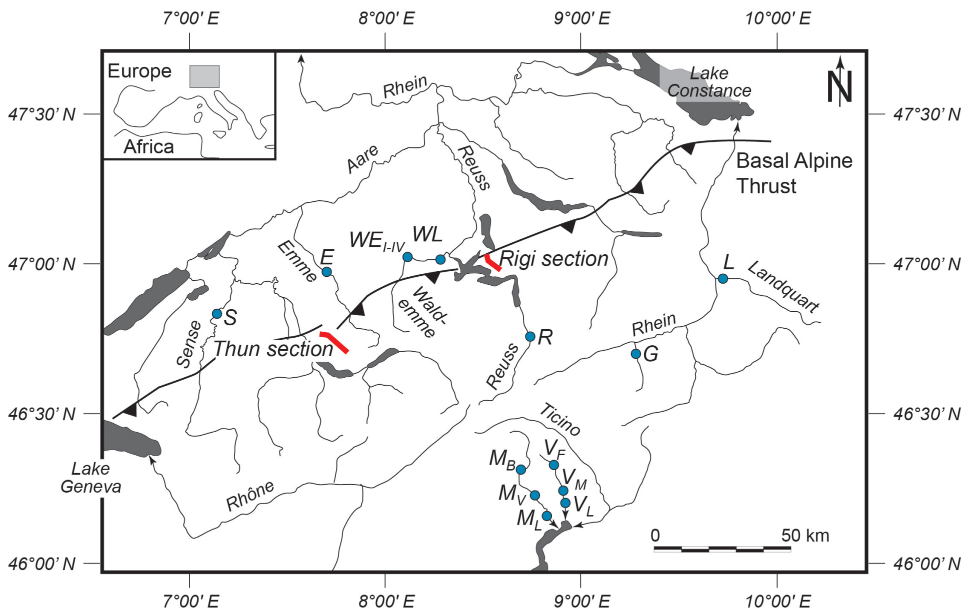

Figure 2

Earth Surf. Dynam. Discuss., https://doi.org/10.5194/esurf-2018-35
Manuscript under review for journal Earth Surf. Dynam.
Discussion started: 3 May 2018

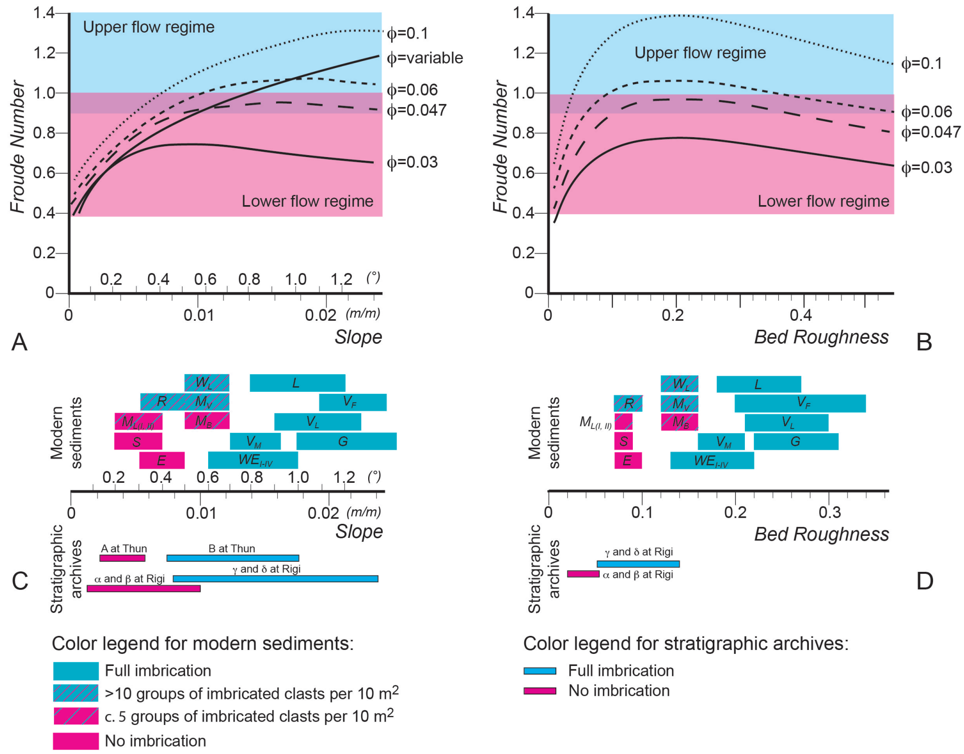

Figure 3

Earth Surf. Dynam. Discuss., https://doi.org/10.5194/esurf-2018-35
Manuscript under review for journal Earth Surf. Dynam.
Discussion started: 3 May 2018

Figure 4

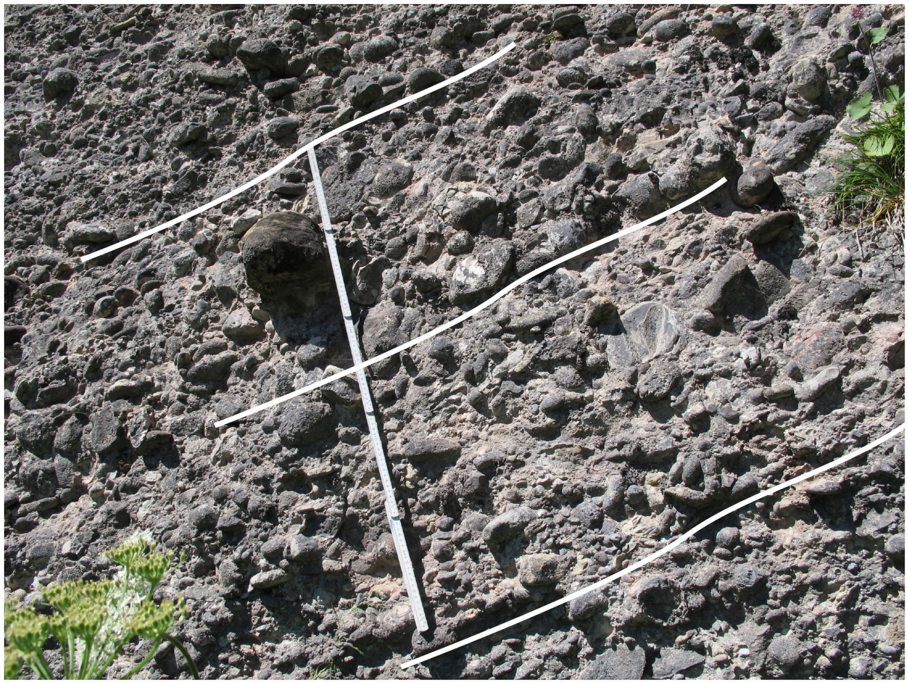

E

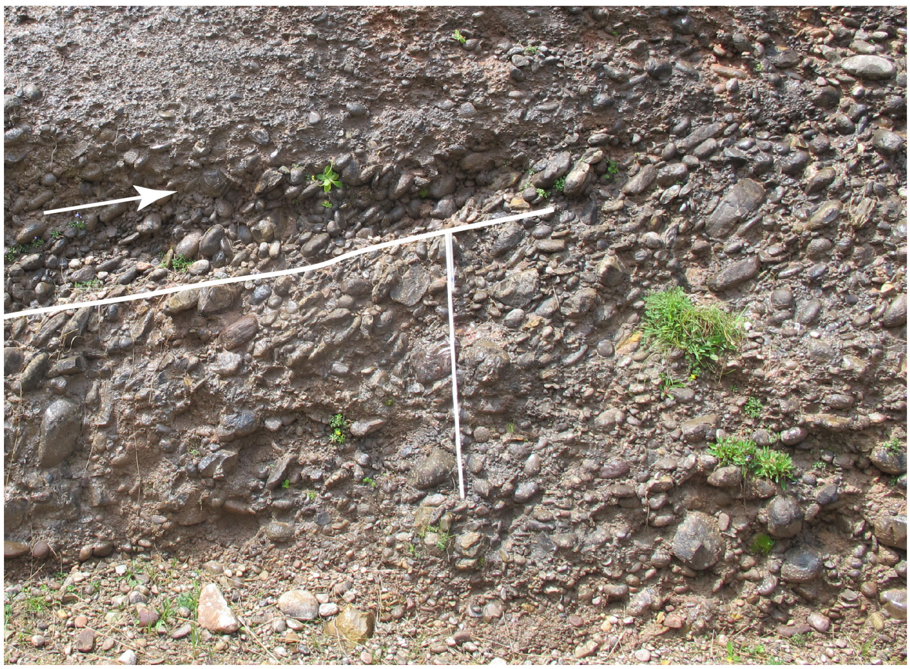

F

Figure 4 (continued)

Earth Surf. Dynam. Discuss., https://doi.org/10.5194/esurf-2018-35
Manuscript under review for journal Earth Surf. Dynam.
Discussion started: 3 May 2018

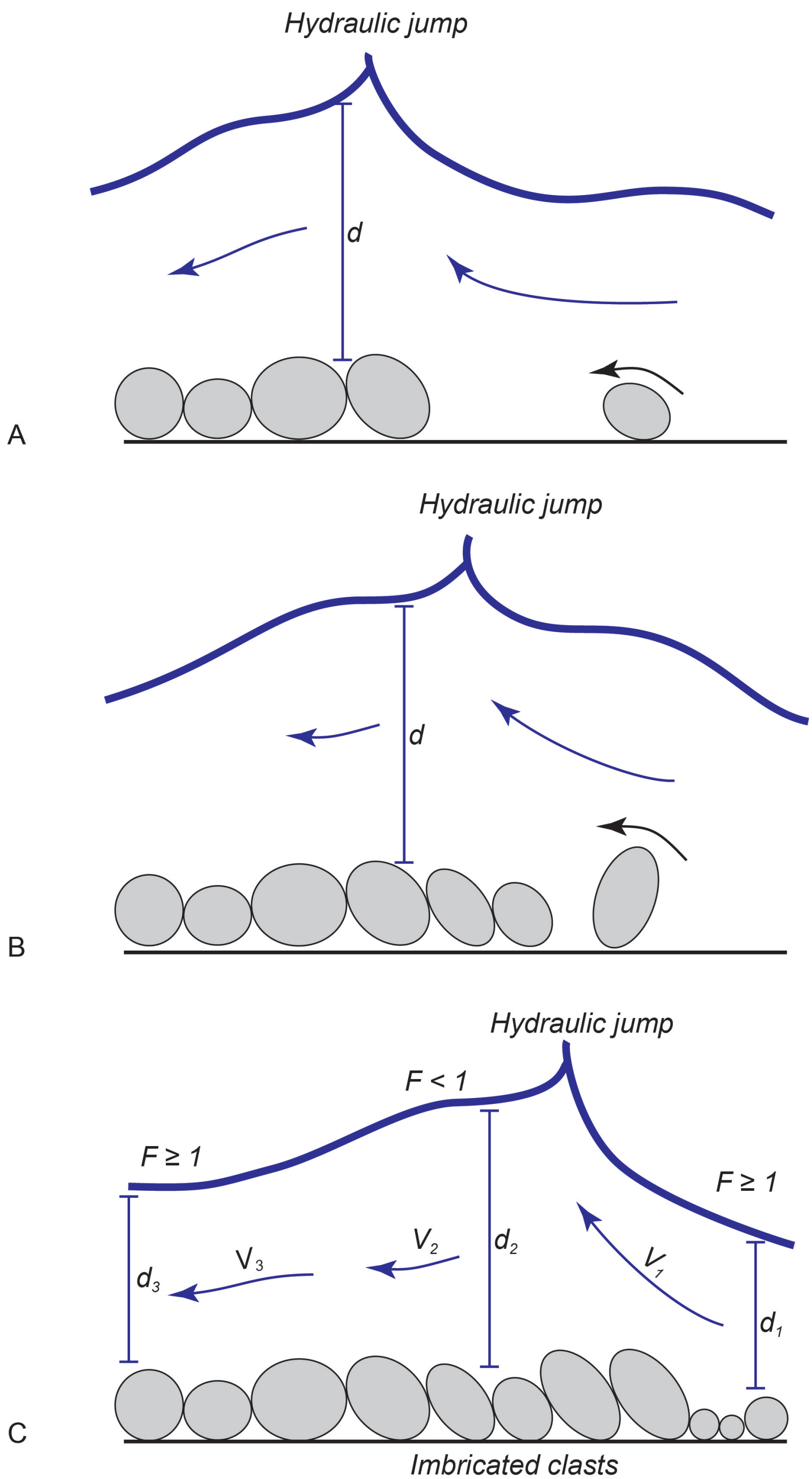

Figure 5

Earth Surf. Dynam. Discuss., https://doi.org/10.5194/esurf-2018-35
Manuscript under review for journal Earth Surf. Dynam.
Discussion started: 3 May 2018

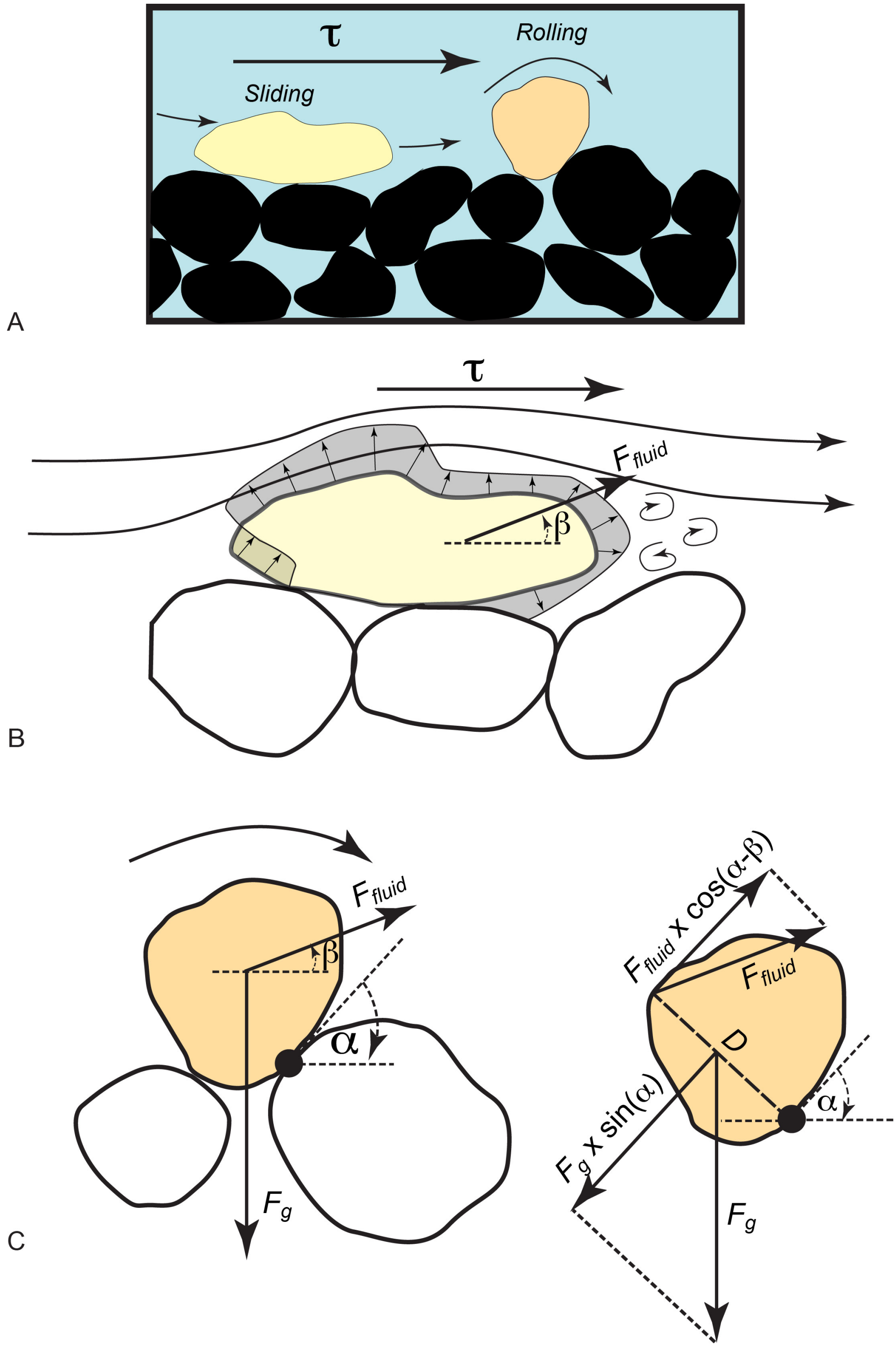

Figure 6

Earth Surf. Dynam. Discuss., https://doi.org/10.5194/esurf-2018-35
Manuscript under review for journal Earth Surf. Dynam.
Discussion started: 3 May 2018

Modern gravel bars

Site name	*Abbreviation*	*Site coordinates*	*D84 (cm)*	*Gradient (m/m)*	*Gradient (°)*	*Inferred water depth d (m)*	*Roughenss*	*Imbrication*
Emme	E	46°57'08N / 7°44'59E	2.3	0.005-0.008	0.4±0.1	0.5-0.8	0.07-0.10	mostly no
Glenner	G	46°44'42N / 9°13'04E	12	0.017-0.024	1.2±0.2	0.4-0.6	0.22-0.31	mostly yes; largest boulders imbricated; smaller pebbles deposited in-between without preferred orientation, sand covers the clast fabric
Landquart	L	46°57'08N / 7°44'59E	10	0.014-0.021	1.0±0.2	0.4-0.6	0.18-0.27	yes
Maggia Bignasco	MB	46°44'42N / 9°13'04E	2.7	0.009-0.012	0.6±0.1	0.2	0.12-0.16	mostly no, but triplets of imbracted clasts occur in places as inferred from photos
Maggia Visletto	MV	46°58'26N / 9°36'29E	9.5	0.009-0.012	0.6±0.1	0.3-0.5	0.12-0.16	partly yes
Maggia Losone I	ML I	46°20'08N / 8°36'25E	4	0.005-0.007	0.3±0.1	0.5-0.6	0.07-0.09	triplets and quadruplets of imbricated clasts occur in places
Maggia Losone II	ML II	46°18'30N / 8°36'35E	6	0.005-0.007	0.3±0.1	0.7-1.0	0.07-0.09	triplets and quadruplets of imbricated clasts occur in places
Verzasca Frasco	VF	46°10'46N / 8°45'33E	2.5	0.015-0.026	1.3±0.2	0.1	0.20-0.34	imbricated
Verzsca Motta	VM	46°10'15N / 8°46'10E	4.3	0.012-0.016	0.9±0.2	0.2-0.3	0.16-0.21	largest boulders imbricated smaller pebbles deposited in-between withour preferred orientation, finer-grained bedforms show imbricated clasts where no boulders are present
Verzasca Lavartezzo	LV	46°20'20N / 8°48'03E	5	0.016-0.023	1.1±0.2	0.2-0.3	0.21-0.30	largest boulders imbricated smaller pebbles deposited in-between without orientation as inferred from photos
Reuss		46°16'28N / 8°48'34E	3.2	0.005-0.008	0.4±0.1	0.3-0.5	0.07-0.10	to large extents yes,triplets and quadruplets of imbricated clasts occur in places. Stream shows standing waves and hydraulic jumps in steep reaches and lower flow regime conditions in flat segments
Sense		46°15'21N / 8°50'23E	6	0.005-0.007	0.3±0.1	0.7-1.0	0.07-0.09	mostly no; imbrications only at the steep downstream slip faces of transerves bars
Waldemme Littau	WL	46°48'53N / 8°39'16E	3.5	0.009-0.012	0.6±0.1	0.2-0.3	0.12-0.16	triplets and quadruplets of imbricated clasts occur in places
Waldemme Entlebuch I	WE I	46°53'20N / 7°20'56E	3	0.01-0.017	0.8±0.2	0.1-0.2	0.13-0.22	yes
Waldemme Entlebuch II	WE II	47°03'04N / 8°15'13E	8	0.01-0.017	0.8±0.2	0.4-0.6	0.13-0.22	yes
Waldemme Entlebuch III	WE III	47°01'57N / 8°04'03E	5.7	0.01-0.017	0.8±0.2	0.3-0.5	0.13-0.22	yes
Waldemme Entlebuch IV	WE IV	47°01'57N / 8°04'03E	8.2	0.01-0.017	0.8±0.2	0.4-0.7	0.13-0.22	yes

Stratigraphic archives

Rigi conglomerates

Segment	*D84 (m)*	*Slope (m/m)*	*Slope (°)*	*Inferred water depth d (m)*	*D84/d*	*Imbrication*
δ	0.07-0.12	0.009-0.027	0.9±0.4	1.2±0.35	0.05-0.14	yes, in places
γ	0.06-0.1	0.008-0.015	0.65±0.2	1.2±0.4	0.04-0.12	partly yes
β	0.04-0.06	0.005-0.01	0.4±0.2	1.7±0.5	0.02-0.05	no
α	0.04-0.06	0.002-0.005	0.2±0.06	2.5±0.8	0.02-0.04	no

Thun conglomerates

Unit	*D84 (m)*	*Slope (m/m)*	*Slope (°)*	*Inferred water depth d (m)*	*D84/d*	*Imbrication*
B	not availble	0.008-0.017	0.72±0.3	1.5-3	not availble	yes, in places
A	not available	0.003-0.005	0.23±0.1	3-5	not availble	no

Table 1